Postprint of: Niedziałkowski P., Bojko M., Ryl J., Wcisło A., Spodzieja M., Magiera Mularz K., Guzik K., Dubin G., Holak T., Ossowski T., Rodziewicz-Motowidło S., Ultrasensitive electrochemical determination of the cancer biomarker protein sPD-L1 based on a BMS-8-modified gold electrode, BIOELECTROCHEMISTRY, Vol. 139 (2021), 107742, DOI: 10.1016/j.bioelechem.2021.107742

© 2021. This manuscript version is made available under the CC-BY-NC-ND 4.0 license http://creativecommons.org/licenses/by-nc-nd/4.0/

Ultrasensitive electrochemical determination of the cancer biomarker sPD-L1 protein based on BMS-8 modified gold electrode

Paweł Niedziałkowski[a]*, Magdalena Bojko[b], Jacek Ryl[c], Anna Wcisło[a], Marta Spodzieja[b], Katarzyna Magiera-Mularz[d], Katarzyna Guzik[d], Grzegorz Dubin[ef], Tadeusz A. Holak[d], Tadeusz Ossowski[a], Sylwia Rodziewicz-Motowidło[b]

[a]Department of Analytical Chemistry, Faculty of Chemistry, University of Gdansk, Wita Stwosza 63, 80-308 Gdansk, Poland

[b]Department of Biomedical Chemistry, Faculty of Chemistry, University of Gdansk, Wita Stwosza 63, 80-308 Gdansk, Poland

[c]Department of Electrochemistry, Corrosion and Materials Engineering, Faculty of Chemistry, Gdansk University of Technology, Narutowicza 11/12, Gdansk, 80-233, Poland

[d]Faculty of Chemistry, Jagiellonian University, Gronostajowa 2, 30-387 Krakow, Poland

[e]Malopolska Centre of Biotechnology, Jagiellonian University, Gronostajowa 7A, 30-387 Krakow, Poland;

[f]Faculty of Biochemistry, Biophysics and Biotechnology, Jagiellonian University, Gronostajowa 7, 30-387 Krakow, Poland

*Corresponding authors, e-mail:

pawel.niedzialkowski@ug.edu.pl

Abstract

Soluble form of Programmed Death - Ligand 1 (sPD-L1) is one of the immune checkpoint proteins which can be detected in the sera of patients with many types of cancer. Taking advantage of the BMS-8 compound properties to create a strong complex with PD-L1 protein, we established a novel biosensing interface detecting sPD-L1. This work describes the chemical modification of gold electrode with BMS-8 compound which interacts with PD-L1 protein. The results show that we can confirm the presence of the sPD-L1 protein in the concentration range of 10^{-18} to 10^{-8} M using electrochemical impedance spectroscopy (EIS) with a limit detection (LOD) of 1.87×10^{-14} M for PD-L1 (S/N=3.3) and at the concentration of 10^{-14} M by cyclic voltammetry (CV).

Additionally, the high-resolution X-ray photoelectron spectroscopy (XPS), contact angle, and surface free energy measurements were applied to confirm the successful functionalization of electrode. Moreover, we investigated the selectivity of the obtained electrode for other proteins, Programmed Death - 1 (PD-1), Cluster of Differentiation 160 (CD160), and the B- and T-Lymphocyte Attenuator (BTLA) in a concentration of 10^{-8} M.

Differentiation between of PD-L1 and PD-1 was achieved on the basis of study of frequency dispersion of capacitance effect at the surface of the modified Au electrode with BMS-8 after incubation in at various concentrations of PD-L1 and PD-1 protein in the range of 10^{-18} to 10^{-8} M. The significant differences are observed in the heterogeneity of PD-L1 and PD-1 measured at the same concentrations of both proteins. The results of quasi-capacitance studies demonstrate that BMS-8 strongly and specifically interacts with PD-L1 protein.

MOST WIEDZY Downloaded from mostwiedzy.pl

Keywords: cysteamine, sPD-L1 protein, gold electrode modification, cyclic voltammetry (CV), Electrochemical Impedance Spectroscopy (EIS).

MOST WIEDZY Downloaded from mostwiedzy.pl

1. Introduction

Every year the number of cancer cases is increasing and only in 2018, 18 million new cases were diagnosed [1]. The cancer treatments are more effective if applied in the early stages of the disease. In tumor diagnosis, many different methods are used, i.e. imaging tests, genetic testing, and measurements of tumor biomarkers [2]. The last of them is the simplest and the least invasive. The early stage of cancer is often correlated with low levels of molecular biomarkers which are difficult to detect. The series of cancer-related biomarkers are used for early diagnosis and are connected with specific cancer, e.g. carbohydrate antigen 125, prostate-specific antigen, alpha fetoprotein, carbohydrate antigen 15-3, carbohydrate antigen 19-9, carcinoembryonic antigen [3–5].

Programmed death - ligand 1 (PD-L1) protein and its receptor, programmed death - 1 (PD-1), are transmembrane, immune checkpoint proteins responsible for the negative regulation of the immune system. PD-L1 also occurs in the soluble form secreted into the serum (sPD-L1) by monocytes, macrophages, and DC [6,7] and is often overexpressed by tumor cells. Moreover, larger amount of soluble form of PD-L1 protein is detected in the sera of patients with malignant melanoma [7], renal carcinoma, nasal natural killer/T-cell lymphoma [8,9], diffuse large B-cell lymphoma [10], myeloma [11], and hepatocellular carcinoma [10]. High level of sPD-L1 impacts overall survival and is associated with the increased mortality in cancer patients [6,9,12]. It is reported that tumor-secreted sPD-L1 is biologically active and able to deliver immunosuppressive signals to lymphocyte T sPD-L1 may be a potential biomarker for anti-PD-1/anti-PD-L1 therapy [7,13].

Currently, the diagnostic tests for PD-L1 which were approved by the Food and Drug Administration relay on immunohistochemistry (IHC). PD-L1 expressed in the tumor tissue is detected by antibodies. IHC-based tests have multiple complicating factors. Among other,

MOST WIEDZY Downloaded from mostwiedzy.pl

different IHC tests use a variation of anti-PD-L1 antibodies with diverse percentage ratio cut-off of the PD-L1 expression level for each test [14,15]. PD-L1 expression is heterogeneous in the tumor tissue and the binding sites for antibodies are limited, what combined with the analysis of biopsies specimens embedded in parafilm (FFPE) provides poorly conclusive results. IHC-approved tests cannot be compared one to another and require standardization and validation [16–18]. Additionally, enzyme-linked immunosorbent assays (ELISA) using sPD-L1 are developed but as in case of IHC test they have different detection range and apply different types of antibodies to detect sPD-L1 protein [19–27]. The comparison of different ELISA tests used for sPD-L1 detection is presented in table S1 in Supporting Information file. This situation provides a burning need to develop reliable diagnostic tests for PD-L1 protein detection what was the aim of our studies.

In the presented study, we developed the electrochemical biosensor for the detection of sPD-L1 protein and we performed a series of experiments confirming its effectiveness and sensitivity. BMS-8 (Bistrol-Myers Sqibb – compound 8; 1-[[3-bromo-4-[(2-methyl [1,1'-biphenyl]-3-yl)methoxy]phenyl]methyl]-2-piperidinecarboxylic acid) molecule was used as a ligand covering surface of gold electrodes [23,24]. The interaction between BMS-8 and PD-L1 was confirmed by co-crystal structure (PDB: 5J8O) and thoroughly tested using Structure-activity relationship by nuclear magnetic resonance spectroscopy (SAR-by-NMR) approach while NMR excluded BMS-8 interaction with PD-1 [28]. The electrochemical studies using gold electrodes modified with BMS-8 enabled the detection of PD-L1 protein at various concentrations in the range of 10^{-18} to 10^{-8} M by EIS technique and at the concentration of 10^{-14} M by CV. We used the high-resolution X-ray photoelectron spectroscopy (XPS) to confirm the modification of gold electrodes. The electrodes were also characterized by the contact angle and surface free energy (SFE) measurements. The selectivity of presented test

MOST WIEDZY Downloaded from mostwiedzy.pl

towards other immune checkpoint proteins: PD-1, cluster of differentiation 160 (CD160), and the B- and T-lymphocyte attenuator (BTLA) has been also investigated.

MOST WIEDZY Downloaded from mostwiedzy.pl

2. Materials and methods

2.1. Chemicals and reagents

All solvents and reagents were used without further purification. 0.1 M phosphate buffer solution (PBS), pH 7.0 was obtained according to the procedure described in [29]. 0.01 M of PBS was prepared from tablets purchased from Sigma-Aldrich, dissolved in ultrapure water, and adjusted to pH 7.0 using 0.1 M hydrochloric acid and pH electrode. N-hydroxysuccinimide (NHS), 1-Ethyl-3-(3-dimethylaminopropyl)carbodiimide (EDC), cysteamine, bovine serum albumin (BSA) were purchased from Sigma-Aldrich. Ethanol, dimethyl sulfoxide (DMSO), potassium ferricyanide $K_3[Fe(CN)_6]$, potassium ferrocyanide $K_4[Fe(CN)_6]$ were purchased from POCh (Poland). The BMS-8 was synthesized as described previously [24,30].

PD-1 and PD-L1 proteins were expressed and purified as described previously [30]. The recombinant human BTLA and CD160 proteins were purchased from Novoprotein, USA (company product code: C563) and ACROBiosystems, USA (company product code: BY5-H5229), respectively.

2.2. EIS and CV measurements

All electrochemical measurements were performed on MultiAutolab M204 potentiostat (Metrohm, Netherlands) using three electrode system. The modified gold electrodes (1.6 mm diameter) were used as working electrodes, Ag/AgCl (0.1 M NaCl) was used as a reference electrode, and platinum wire was used as an auxiliary electrode.

The cyclic voltammetry measurements were conducted in the solution consisting of the equimolar amounts of 1 mM $K_3[Fe(CN)_6]$ and $K_4[Fe(CN)_6]$ dissolved in 0.1 M PBS, pH 7.0. Before each measurement, the solution was purged with nitrogen to remove oxygen. All

MOST WIEDZY Downloaded from mostwiedzy.pl

cyclic voltammograms were recorded in the potential range of - 0.6 V to 0.8 V with the scan rate of 100 mV/s.

The electrochemical impedance spectroscopy analyses were performed to evaluate BMS-8/Au sensor efficiency and selectivity. All measurements were performed at room temperature in the same conditions and solutions as in CV measurements using Nova 1.1 software. The analysis was carried out using Frequency Response Analyzer (FRA) implemented in MultiAutolab M204 potentiostat. The measurements were carried out in the potentiostatic mode at formal potential. The perturbation amplitude was 10 mV. The studied frequency range was set between 10 kHz and 0.1 Hz in the descending order. The EIS data were analyzed using dedicated software with NelderMead algorithm developed in LabView environment [31].

2.3. X-Ray Photoelectron Spectroscopy (XPS) measurements

X-Ray Photoelectron Spectroscopy (XPS) analysis was carried out using Escalab 250Xi spectroscope (ThermoFisher Scientific, United Kingdom). The spectroscope was equipped with Al Kα monochromatic X-Ray source, 250 μm spot diameter. The applied pass energy was 15 eV. Charge compensation was controlled through low-energy Ar^+ ions emission by means of a flood gun, with the final calibration made with reference to the gold substrate (BE +84.0 eV) [32]. Deconvolution procedure was performed using Avantage software provided by the manufacturer. XPS analysis were performed using gold on glass substrates (11 mm × 11 mm) (Arrandee, Werther, Germany) modified in the same way as electrodes for electrochemical measurements.

2.4. Contact angle and surface free energy (SFE) measurements

MOST WIEDZY Downloaded from mostwiedzy.pl

The contact angle and surface free energy were measured using Drop Shape Analyzer — DSA100 by Krüss. The contact angles of drops of four different liquids (water, formamide, glycerol, and diiodomethane) were measured to determine the surface free energy. The image of a 4 μL drop of the probe liquid deposited using a syringe was captured by a CCD camera connected to a graphics card. The measurements were repeated 20 times. After the digital image analysis, the average contact angle was deduced using the Young-Laplace method from the angles measured at both sides of the drop in equilibrium. The total surface free energy γs and its dispersive γd and polar γp components of the surfaces were determined by the Owens, Wendt, Rabel, and Kaelble (OWRK) method from the contact angles of the four liquid drops. In addition, the polar components were expressed as their acid γ+ and basic γ− components by the van Oss and Good method; γ+ and γ− reflect the donor and acceptor characters of the surface [33–36].

2.5. Modification of bare Au electrode by cysteamine and BMS-8

The bare gold electrodes before each modification by cysteamine were polished with 1 μm and then with 0.05 μm alumina slurry. Afterward, the electrodes were rinsed twice with distilled water and then with 0.01 M PBS, pH 7.0, and dried in a stream of nitrogen. All electrodes before modification were electrochemically tested by CV and EIS measurements.

In the first step of modification, the electrodes were covered by formation of self-assembled monolayer (SAM) of cysteamine at the electrode surface. The gold electrodes were immersed in 5 mL of 0.018 M cysteamine solution dissolved in 99.8 % of ethanol for 12 h at 4 °C. Subsequently, the gold electrodes were thoroughly rinsed with ethanol, then by 0.01 M PBS, pH 7.0, and water to remove the residual amount of cysteamine. Subsequently, the electrodes after drying in the stream of nitrogen were used for the modification with BMS-8.

MOST WIEDZY Downloaded from mostwiedzy.pl

The procedure for the modification of the gold electrodes with BMS-8 consisted of two steps. In the first step BMS-8 was dissolved in 2 mL of DMSO to obtain 5 mM solution. The obtained solution was then added to the 2 mL vessel of the previously prepared mixture of 0.1 M of EDC, 0.05 M of NHS and 100 μM of trimethylamine in DMSO. Secondly, after 1 h the gold electrodes previously modified with cysteamine were placed in the EDC/NHS/BMS-8 mixture for 16 h at room temperature. Described procedure of BMS-8 immobilization is characterized by very high reproducibility on gold electrodes as well as on various gold substrates.

2.6. Preparation of the modified Au electrodes for the electrochemical detection of PD-L1 protein

The modified gold electrodes after incubation in BMS-8 solution were rinsed thoroughly with 0.01 M PBS, pH 7.0 and deionized water. Then, the electrodes were dried in a stream of nitrogen. In order to investigate the influence of blocking the nonspecific binding sites occurring on the surface we tested two approaches, the electrodes were incubated in 10 μL of 1 % BSA solution in 0.01 M PBS, pH 7.0, for 30 min and the step of incubation in 1 % BSA was omitted. In the case of measurements without using BSA electrode were incubated in solution containing 2 mM 1-hexanethiol for 30 min. Then, the electrodes were incubated in various concentrations of PD-L1 protein - in 10^{-18} to 10^{-8} M concentration range and in 10^{-14} M in the case of EIS and CV measurements, respectively. The deposition process was performed by dropping 10 μL of protein in 0.01 M PBS, pH 7.0 onto the electrode surface and incubation for 1 h. Modified electrodes were rinsed with deionized water and 0.01 M PBS, pH 7.0 before each measurement. Additionally, the test of influence of 0.01 M PBS, pH 7.0 (incubation for 1h) on the electrode was performed.

MOST WIEDZY Downloaded from mostwiedzy.pl

3. Results and discussion

3.1. Preparation of the electrode sensitive towards PD-L1 protein

The detection of PD-L1 protein was conducted by anchoring of BMS-8 onto the gold electrode surface, previously modified with cysteamine. The modification procedure of the first monomolecular layer used in this work was described previously [37]. This procedure was modified by change of the solvent from water to ethanol. The modification of the gold electrodes was performed in 18 mM solution of cysteamine in 99.8 % ethanol during 12 h. Many authors have performed the incubation of electrodes in aqueous solution during 4 or more hours using various concentrations of cysteamine in aqueous solution [38–43]. There are also some reports of the gold electrode modification in the ethanolic solution [44,45]. The previous work proved that there are no significant differences in the formation of monolayer for the cysteamine dissolved in water or ethanol [46]. The modification of electrodes with BMS-8 was performed in the anhydrous conditions using DMSO due to the better solubility of BMS-8 in this solvent. The chemical reaction was carried out by prior activation of BMS-8 carboxylic group performed in the mixture of EDC/NHS [47].

The carboxylic group of BMS-8 forms an amide bond with the amine group of cysteamine anchored on the electrode. It is worth noting that the carboxylic group of BMS-8 is not essential for the interaction of the compound with PD-L1 protein [30]. Therefore, BMS-8 anchored onto the electrode surface by amide bond maintains its activity.

During performed experiments the non-specific binding spots occurring on the surface of the electrode were not blocked by BSA, however the influence of 1% BSA in 0.01 M PBS, pH 7.4 on the electrode behavior after modification was also tested. Electrodes obtained in this procedure were subsequently used to examine various concentrations (in the range of 10^{-18} to 10^{-8} M) of PD-L1 protein. Each step of electrode preparation and chemical structure of

MOST WIEDZY Downloaded from mostwiedzy.pl

BMS-8 is shown in Figure 1 A. The detection of PD-L1 protein concentration is based on the modulated charge transfer kinetics, in presence of the redox species, after PD-L1 is anchored on the functionalized electrode surface. All steps of the modification and detection of examined proteins were characterized by changes in EIS and CV measurements. The same procedure as described above was performed for the study of interaction of obtained electrodes with PD-1 protein in the range of concentration from 10^{-18} to 10^{-8} M and BTLA and CD 160 in the concentration of 10^{-8} M.

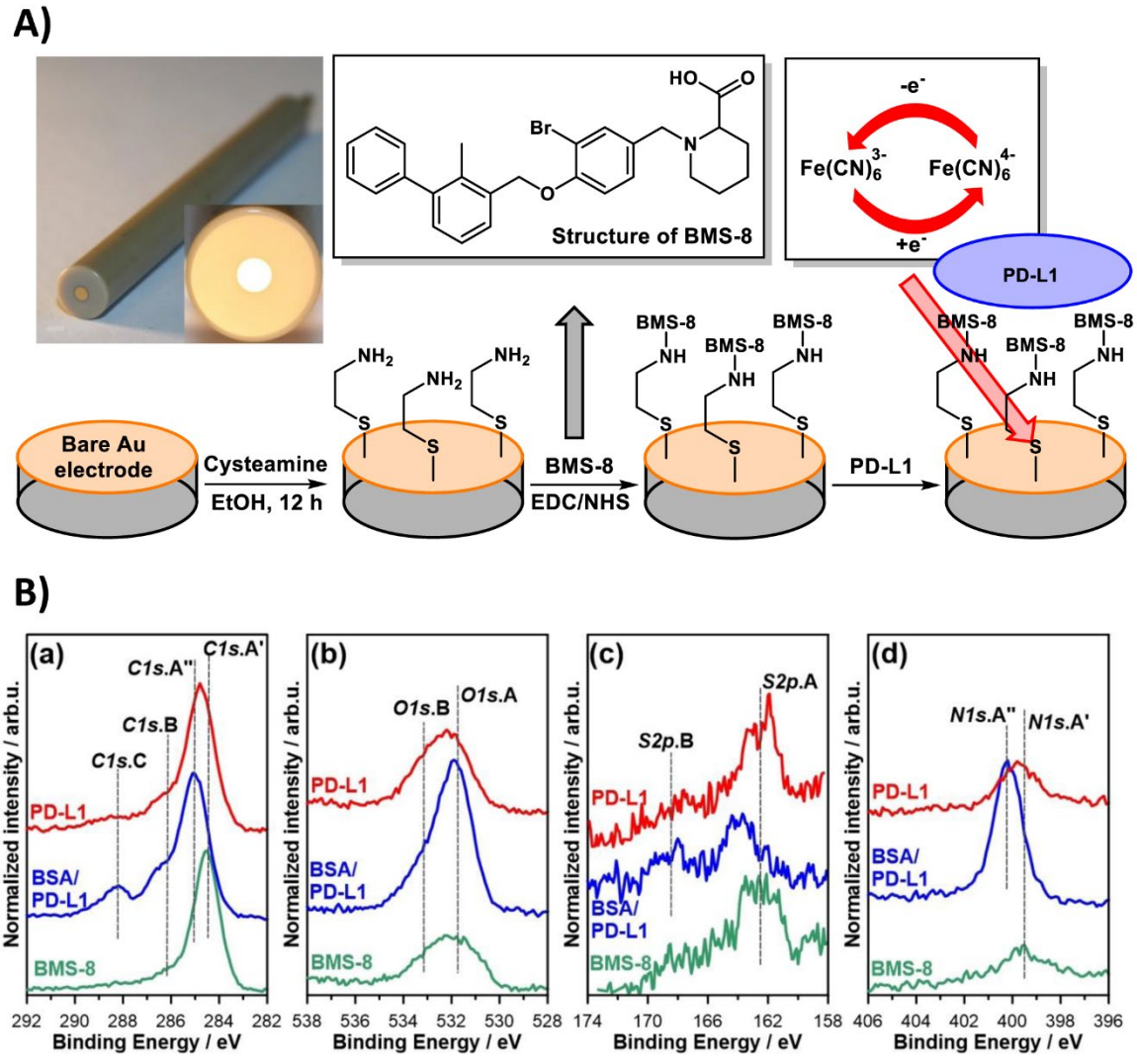

Fig 1. A) The picture of gold electrode and the procedure of its modification by cysteamine and BMS-8. B) High-resolution XPS spectra obtained in the binding energy range of: (a) *C1s*, (b) *O1s*, (c) *S2p,* and (d) *N1s* photopeaks.

MOST WIEDZY Downloaded from mostwiedzy.pl

3.2. XPS measurements during each step of gold electrode modification process

Figure 1B presents the results of the high-resolution XPS analysis conducted on the surface of functionalized Au electrodes in the energy range of *C1s*, *O1s*, *S2p,* and *N1s* peaks. The analysis was also carried for *Au4f* peak doublet, which served as a reference for the peak calibration and the indicator of the acquired functionalization thickness.

The primary component reported in *C1s* spectrum (Fig. 2a) — *C1s*.A — is located at 284.6 ± 0.1 eV for BMS-8 and PD-L1 samples but exhibits even more positive shift towards 285.1 eV for BSA+PD-L1 samples. The peaks located at this binding energy range are typically attributed to various aliphatic hydrocarbon species but can also originate from adventitious carbon contamination due to air exposure. The second notable component — *C1s*.B — is shifted s shifted versus the primary *C1s* component by approx. +1.6 eV and originates from C-O and C-N bonds found in hydroxyls, esters, amines, and others. The last component *C1s*.C was observed at approx. 288.2 eV in an energy range most often associated with carboxyl functional groups. The contribution of the last component is distinctly more prominent for BSA/PD-L1 samples, where its share in total carbon content is approx. 25% versus 15% for PD-L1 samples and 7% for BMS-8. The details of the peak decomposition are summarized in Table 1. The applied model is consistent with numerous literature reports [48–52].

Table 1. Results of high-resolution XPS analysis and peak deconvolution

	C1s			*O1s*		*S2p*		*N1s*	*Au4f*
	C1s.A	*C1s*.B	*C1s*.C	*O1s*.A	*O1s*.B	$S2p_{3/2}$.A	$S2p_{1/2}$.B	*N1s*.A	--
BE / eV	284.6*	286.2	288.2	531.6	532.8	164.5	167.7	399.7**	84.0
BMS-8	41.2	7.6	3.5	3.5	3.7	2.8	1.1	3.5	33.1
BSA/PD-L1	40.2	11.1	11.3	7.0	7.3	1.8	1.0	9.1	11.2
PD-L1	36.7	10.1	5.7	4.0	5.9	2.6	0.9	4.5	29.6

* *C1s*.A peak was equal 285.0 eV for both BSA/PD-L1 samples.

** *N1s*.A peak was equal 400.2 eV for both BSA/PD-L1 samples.

MOST WIEDZY Downloaded from mostwiedzy.pl

The presence of carbon-oxygen bonds, which are characteristic for organic compounds, was further confirmed based on *O1s* peak analysis (Fig. 2b) where the presence of C-O/OH and C=O bonds is reflected in the photopeaks located at *O1s*.A = 531.6 eV and *O1s*.B = 532.8 eV, respectively. The lowest amount of oxygen in the BMS-8 sample corresponds to the smallest share of *C1s*.B and *C1s*.C peaks during *C1s* spectra analysis [53,54]. XPS analysis carried out in the binding energy range of *N1s* photopeak (N1s.A) resulted in the observation of the significant differences between BSA/PD-L1 and the remaining samples. The *N1s* peak position is shifted by +0.5 eV with respect to BMS-8 and both PD-L1 samples. The position of this peak is most commonly attributed to N-H and N-C bonds in amines [55,56]. The energy shift most likely originates from the different number of carbon atoms adjacent to nitrogen. Indeed, the amount of nitrogen in BSA/PD-L1 samples was over twice higher than in PD-L1 samples. Higher nitrogen content might also be the reason of the *C1s*.A component energy shift (*C1s*.A' and *C1s*.A''). Each analyzed sample contained between 2.5 and 4 at.% of sulfur present in two chemical states. The primary state marked as *S2p*.A is located in the binding energy characteristic for thiols and other organic forms of sulfur, while the second component (*S2p*.B) was significantly smaller and shifted towards BE range typical for sulfates. The XPS analyses allow to bring a conclusion regarding successful electrode surface functionalization with studied proteins.

Finally, the XPS analysis also provides coarse information about the electrode functionalization thickness. The photoelectrons are emitted only from approximately 5-10 nm depth underneath the interface. Two conclusions can thus be drawn. First, the functionalization thickness did not exceed 10 nm in any case, a conclusion drawn based on the presence of *Au4f* peak doublet for metallic gold in the analyzed surface chemical states. Second, the functionalization is thinner in the case of BSA/PD-L1 samples.

MOST WIEDZY Downloaded from mostwiedzy.pl

3.3. Surface wettability measurements

In order to assess the hydrophobic and hydrophilic character of the modified surface at the different steps of the modification process of the gold electrodes, contact angles of water drops deposited on the surfaces were measured (Fig 2, Fig. 3a). For gold electrodes the water contact angle decreased after modification with cysteamine for about 10°. Further modification with BMS-8 led to a decrease in the contact angle for about 12°. The decrease of contact angle on the modified Au electrodes revealed an increase of hydrophilic character of the surface because of the functional groups present in the modified layer. Deposition of BSA on the modified layer leads to another decrease in the contact angle for about 5°. In both cases (with or without the BSA) after exposure to the PD-L1 protein an increase in the contact angle is observed, hence the hydrophobicity of the layer increases (Fig 2, Table S2).

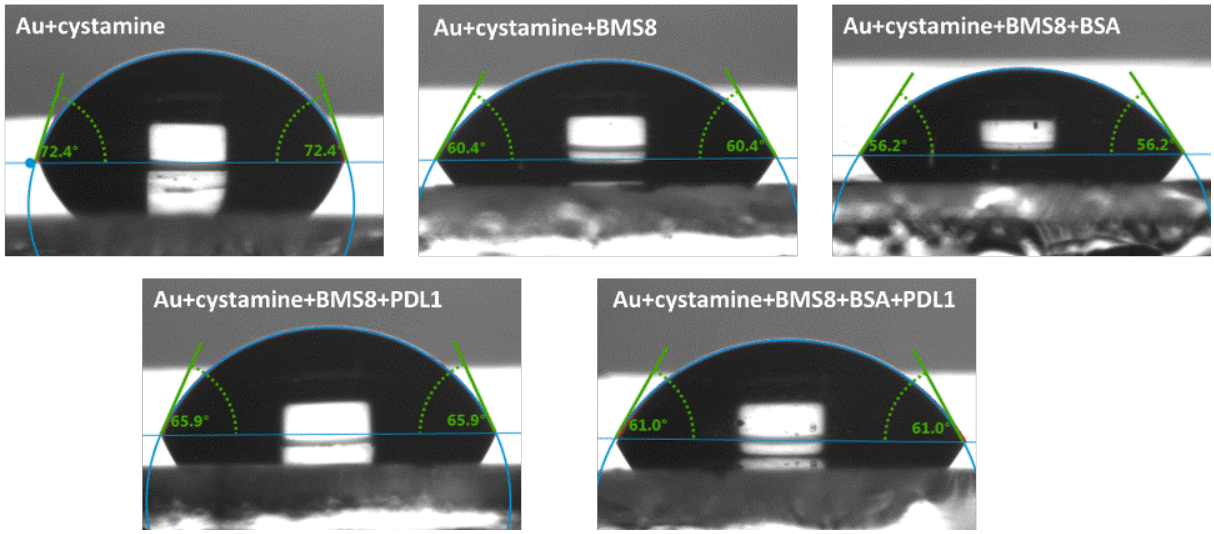

Fig. 2. Photos of the water contact angle measurements for each step of gold electrode modification for PD-L1 sensing.

Considering the changes in SFE energy in relation to the subsequent stages of modification, the total free energy does not change significantly as to the value, while the changes in the chemical structure of the layer also change the SFE value (Fig. 3b). The total

MOST WIEDZY Downloaded from mostwiedzy.pl

SFE and its polar component increased as a result of the incorporation of more functional polar groups due to the modification process. Changes in the free energy of the surface are mainly the effect of the change of the polar component, while the dispersion part remains essentially unchanged.

Already the first stage of modification with cysteamine causes the increase of the acid-base component from 3.09 mN/m to 5.86 mN/m. Furthermore, the acidic and basic elements of the polar component undergo a complete change. In the case of an unmodified electrode, the acid component has a much higher share. The modification process not only lowers their values but also reverses the proportions — the basic component is now dominant. This is probably consistent with the presence of amino groups exhibiting basic properties on the electrode surface. The largest increase in the basic component is observed in the case of BMS-8/BSA and BMS-8/BSA/PD-L1 samples. This observation is consistent with the results obtained from the XPS measurements which indicated these samples as containing the most nitrogen atoms in the form of different types of amino groups.

MOST WIEDZY Downloaded from mostwiedzy.pl

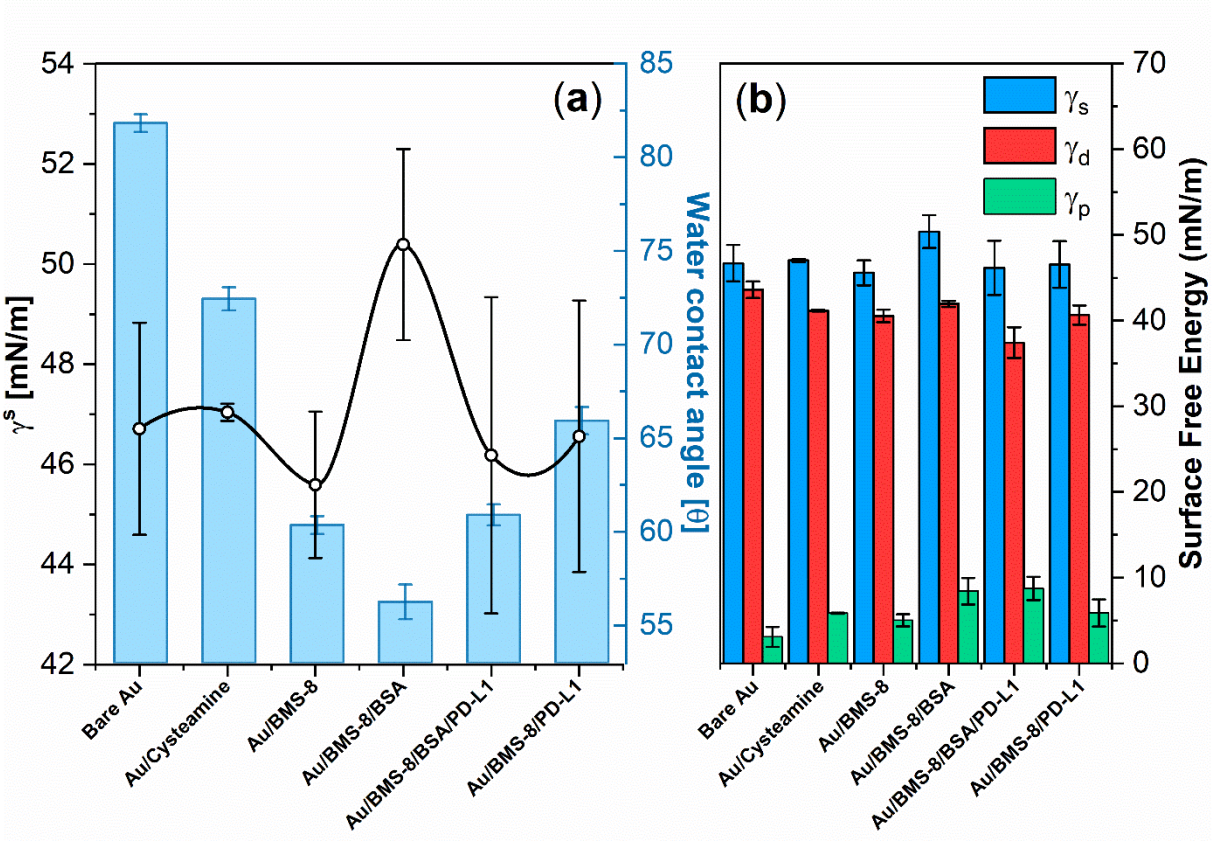

318

319 Fig. 3.a) Water contact angle and b) SFE energy γs diagram with uncertainties for each step of
320 the modification of the gold electrode for PD-L1 sensing.

321

322 This variability affects the hydrophilicity of the surface and thus the observed contact angle.
323 The most hydrophilic surfaces are observed for BMS-8/BSA and BMS-8/BSA/PD-L1
324 samples. Their water contact angle (WCA) decreased from 81.82 for unmodified gold
325 electrode to 56.26 and 60.90 for BMS-8/BSA and BMS-8/BSA/PD-L1, respectively.

326

MOST WIEDZY Downloaded from mostwiedzy.pl

3.4. Electrochemical measurements

The cyclic voltammetry measurements were performed during each step of electrodes modification in 0.1 M of PBS, pH 7.0 containing 1 mM $Fe[(CN)_6]^{3-/4-}$. The results of CV measurements show two reversible peaks for bare Au electrodes, where the ratio of anodic peak to cathodic peak current i_A/i_C is close to 1 with the peak-to-peak separation (ΔE) of 67 mV (Fig. 4. black dotted line). After modification by cysteamine, the peak-to-peak separation ΔE decreased to 64 mV and is similar to those calculated for bare Au electrodes. Therefore, a conclusion may be drawn that cysteamine modification of Au electrodes does not influence significantly its electrochemical behavior, which was also confirmed in our measurements by EIS technique. The voltammogram is shifted towards more negative potential after modification, a feature observed before [44].

The modification with BMS-8 caused the peak currents to decrease and the increase of peak-to-peak separation to 119 mV. In the next step, such modified electrode was incubated with PD-L1 protein in a concentration of 10^{-14} M. The changes of obtained voltammograms are significant. The peak current values decreased, and the peak-to-peak separation increased, ΔE to 180 mV (Fig. 4), as an effect of PD-L1 anchoring at the modified electrode surface and affecting the charge transfer kinetics by the redox species. This particular behavior of the modified electrodes is probably the consequence of two competitive factors: partial blockage of active sites at the electrode and electrostatic interactions between PD-L1 protein and negatively charged ions $Fe[(CN)_6]^{3-/4-}$ present in the examined solution [55,56].

The experiment was performed using gold electrode modified by cysteamine with BMS-8 without incubation with 1% BSA in 0.01 M PBS due to the small changes caused by BSA observed in electrode response in previous experiments (see Fig. S1). Above experiment directly confirm that gold electrode modified by BMS-8 is highly sensitive to PD-L1 protein present in solution.

MOST WIEDZY Downloaded from mostwiedzy.pl

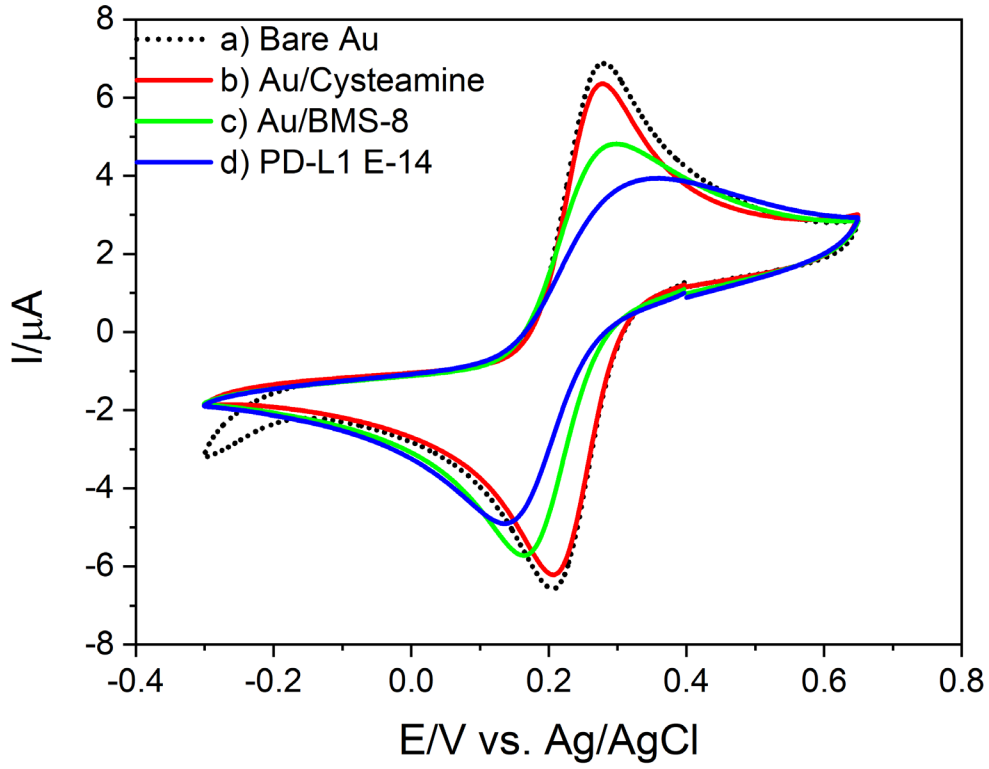

352

353 **Fig. 4.** Cyclic voltammograms of the redox reaction of 1 mM $Fe[(CN)_6]^{3-/4-}$ in 0.1 M PBS, pH
354 7.0 solution obtained at a) Bare Au b) Au/Cysteamine c) Au/BMS-8 d) Au/BMS-8/PD-L1
355 electrode, scan rate 100 mV/s.

MOST WIEDZY Downloaded from mostwiedzy.pl

Next, the electrochemical impedance spectroscopy measurements have been performed to determine the capability of the obtained electrodes for detecting PD-L1 at very low concentrations. Additionally, the electrodes modified with BMS-8 were used as a control test during PD-1 detection. The impedance approach offers significantly higher sensitivity for the determination of electrode kinetics changes in comparison with CV measurements. Therefore, it was selected for the evaluation of both PD-L1 and PD-1 concentrations in the same range of 10^{-18} to 10^{-8} M. Figure 4 presents the EIS impedance spectra for the bare Au electrodes in 0.1 M PBS pH 7.0 solution containing 1 mM $Fe[(CN)_6]^{3-/4-}$, after consecutive surface modification steps and after incubation in solution containing PD-L1 protein in concentration range of 10^{-8} to 10^{-18}.

The shape of the impedance spectra is characterized by the semicircle at the high-to-moderate frequency range and very distinctive feature in the form of solid line inclined at 45° at low-frequency range. The discussed feature should be associated with the diffusion-related impedance and testifies for the co-occurrence of the diffusion control in the charge-transfer process. On the other hand, it is clearly visible in the inset of Fig. 5 that the next electrode modification steps influence the electrode's charge transfer resistance as observed through the increase of the high-frequency semicircle.

The electric equivalent circuit (EEC) was selected based on the obtained impedance studies. The EEC with abbreviated notation R(Q(RW)) is composed of R - solution resistance and a parallel connection of the constant phase element (CPE), imitating the heterogeneities at the electrode surface and charge transfer resistance R_{CT} with Warburg diffusion resistance W (Fig. 5). The impedance of the CPE is given with eq. (1)

$$Z_{CPE} = \frac{1}{Q(j\omega)^{\alpha}} \quad (1)$$

where Q is the quasi-capacitance in the presence of frequency dispersion of capacitance, CPE exponent α is the heterogeneity factor, j is the imaginary number and ω is the angular

MOST WIEDZY Downloaded from mostwiedzy.pl

frequency [57–62]. CPE exponent α is often considered to be the surface heterogeneity factor ($0 < \alpha < 1$). The closer to unity α approaches, the more closely the CPE resembles a pure double-layer capacitance, and if α approaches 0, the CPE behaves more like a resistor. The above-defined heterogeneity may be introduced by numerous features, including non-uniform site-specific charge transfer kinetics due to electrode polycrystallinity, 2D adsorption of macromolecules or contaminants, and resultant interspace regions but also electrode material geometry and porosity [63–69]. The utilization of such electric equivalent circuit is explained due to the large molecular mass of examined proteins and is widely used for the gold electrode modified by cysteamine and other organic molecules [70–74]. The EEC allowed obtaining a very good fit as represented by Chi^2 distribution about 10^{-4}. The more detailed analyses of are summarized in Table S3 in Supporting Information file.

The impedance spectra for both: bare Au electrode and Au after modification with cysteamine reveal nearly straight line at 45° (Fig. 5a inset), a feature characteristic for a mass diffusion limiting the electron transfer process. The electrode modification through a chemical reaction between electrode-terminating amine functional groups with the carboxyls within BMS-8 molecule caused the appearance of a distinctive capacitive semicircle on the impedance spectra, indicating the formation of the adsorbed layer, which influence the interfacial electron transfer.

The BMS-8 surface functionalization process occurs with different efficiency for various electrodes, differing in BMS-8 anchoring density, resulting in differences in layer thickness, and subtle Au pretreatment conditions, etc. These features have a non-negligible influence on the kinetics of the charge transfer through the electrode interface. Therefore, in order to efficiently verify the effect of anchoring the PD-L1 molecule on the modified electrode surface, it is essential to perform the experiment on a single electrode, to be able to observe the relative changes of R_{CT} parameter. The relative change of the charge transfer

MOST WIEDZY Downloaded from mostwiedzy.pl

resistance was calculated according to the equation: $\Delta R_{CT} = R_{CT(PD\text{-}L1)} - R_{CT(BMS\text{-}8)}$, where $R_{CT(BMS\text{-}8)}$ is a value of R_{CT} of electrode modified by BMS-8 and $R_{CT(PD\text{-}L1)}$ is R_{CT} after incubation in different concentration of PD-L1. The obtained results are shown in Fig. 5b.

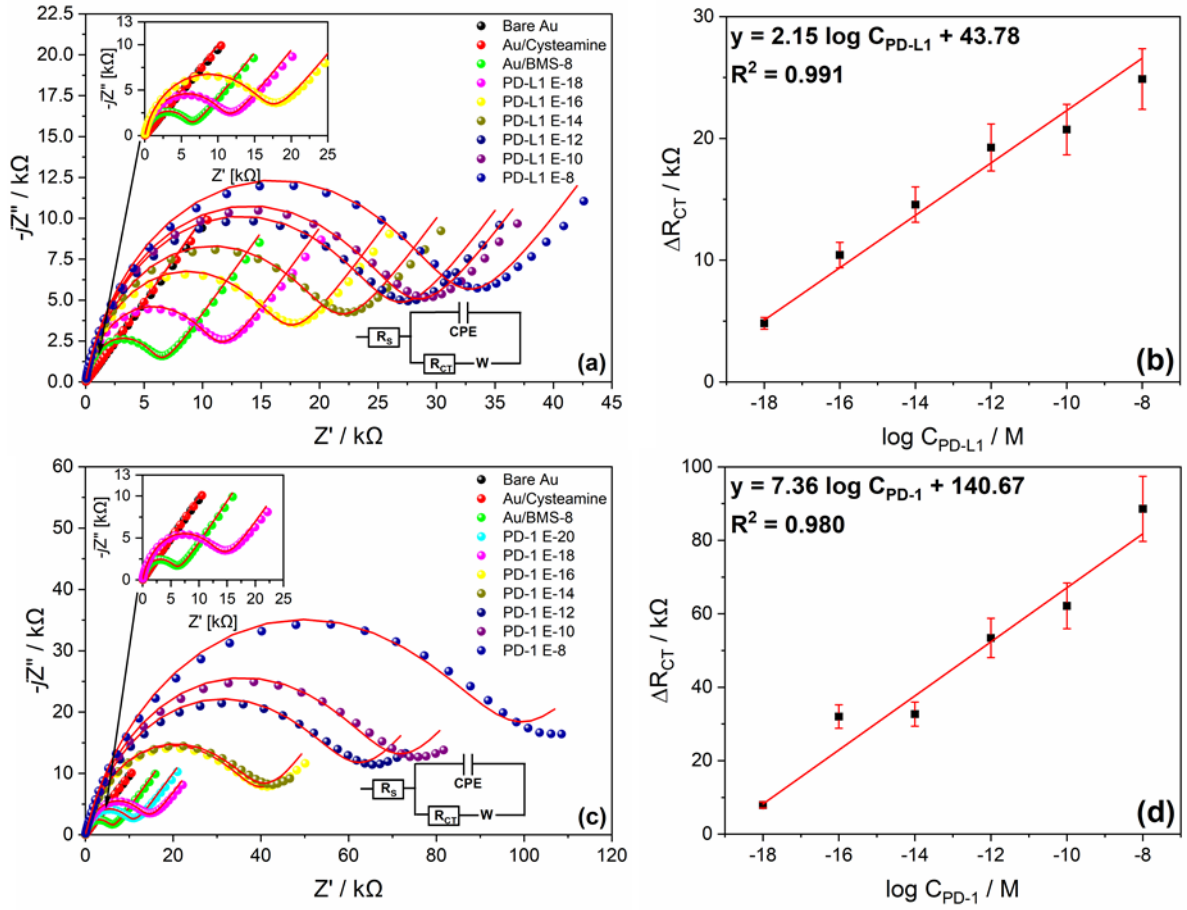

Fig. 5. The EIS impedance spectra of BMS-8 functionalized electrode in the absence and the presence of a) PD-L1 and c) PD-1 protein in 0.01 M PBS, pH 7.0 at various concentrations ratio from 10^{-18} M to 10^{-8} M. In the inset enlarged the comparison of obtained spectra for a) PD-L1 and c) PD-1 concentration of 10^{-18} M. Points represent experimental results while solid red line represent data calculated using EEC.
The calibration curve for the ΔR_{CT} changes resulting from b) PD-L1 and d) PD-1 protein exposure of the electrode as a function of logarithmic concentration of PD-L1.

It is clearly visible that tested BMS-8 deposited at the Au electrode surface is highly sensitive, differentiating impedance characteristics of the electrode even at the lowest studied concentration of PD-L1. These results indicate that studied protein binds to the BMS-8 molecules, anchored on the Au electrode. The increasing protein concentration causes inhibition of the charge transfer process, resulting in R_{CT} increase. The observed behavior

MOST WIEDZY Downloaded from mostwiedzy.pl

corresponds with the formation of the functionalized organic layer affecting the charge transfer kinetics. The EIS studies revealed that the R_{CT} of the above-functionalized electrode increases over 2.5 times in the presence of PD-L1 protein in the vicinity in the concentration of 10^{-18} M to 10^{-8} respectively (Table S4).

Performing the above-described R_{CT} normalization allowed us to form the calibration curve, thus offering the detection tool of ultra-small PD-L1 concentrations on the modified Au surface, based on electrochemical impedance measurements. The electrochemical response of the BMS-8 modified gold electrode was linear in the entire range of the PD-L1 from 10^{-8} M to 10^{-18} M. The calculated regression equation was: $\Delta R_{CT} = 2.15 \log C[PD\text{-}L1] + 43.78$ with the correlation coefficient of 0.991. The detection limit (LOD) was estimated to be 1.87×10^{-14} M and 2.93×10^{-14} M for PD-L1 and PD-1 (S/N=3.3) respectively, while the limit of quantification (LOQ)was calculated to be $5{,}67 \times 10^{-14}$ M for PD-L1 and $8{,}87 \times 10^{-14}$ M for PD-L1.

3.6. Specificity and selectivity of the impedance PD-L1 assay

In order to examine the selectivity of the above-presented approach, the same experiment was performed towards the detection of the PD-1 protein. Obtained results confirm that the presence of PD-1 protein in the analyte has a visible effect on the charge transfer, increasing R_{CT} (Fig. 5c). The results of impedance analyses of PD-1 protein detection are summarized in Table S3. The data plotted in Fig. 5d reveals that the ΔRct changes recorded for the Au/BMS-8 were linear in the range of analyzed PD-1 concentrations, similar as in the case of PD-L1 protein. The estimated regression equation was $\Delta R_{CT} = 7.36 \log C[PD\text{-}1] + 140.67$, with the correlation coefficient equal to 0.980 (Fig. 5d). BMS-8 functionalized electrode response to PD-1 is unexpected given the fact that BMS-8 was shown

MOST WIEDZY Downloaded from mostwiedzy.pl

not to interact with PD-1 [28]. Likely the surface modification process itself provides anchor points for PD-1.

The performed analyses directly indicate the linear trend of ΔR_{CT} change as a function of target protein concentration for both studied proteins. However, there is also a significant difference in the slope of the linear function. The charge transfer resistance through the BMS-8-modified Au electrode increases over 2.5 times in the analyzed concentration range of PD-L1, and over 5.0 times in the same range of PD-1 protein. Thus, a conclusion should be drawn that analysis of this one parameter allows for an ultrasensitive quantitative analysis but does not allow for qualitative analysis distinguishing between PD-1 and PD-L1 proteins.

There are, however, other parameters obtained based on the impedance analyses. An important feature should be observed when analyzing the changes of the quasi-capacitive parameter with the concentration change of either PD-1 or PD-L1 molecules, the results of which are presented in Fig. 6.

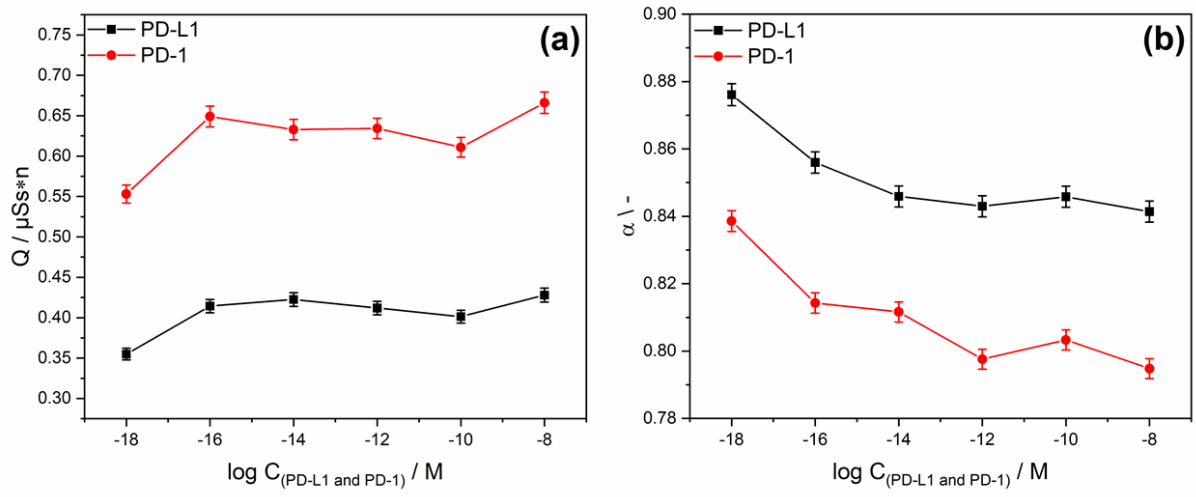

Fig. 6. a) The relationship of a) quasi-capacitance in the presence of frequency dispersion of capacitance (Q) and b) heterogeneity factor (α) as a function of logarithmic concentration of PD-L1 and PD-1 proteins.

MOST WIEDZY Downloaded from mostwiedzy.pl

The quasi-capacitance parameter Q_{DL} increases with analyte concentration for both studied proteins PD-L1 and PD-1, and this effect is strongly correlated with the decrease in CPE exponent α, indicating a slight decrease in electrode homogeneity when more and more target proteins are anchored on the electrode surface. This is an expected and valuable result, confirming the correct selection of the EEC.

The values of the quasi-capacitance of the modified Au electrode exposed to the studied proteins differ significantly. The heterogeneity introduced by the PD-L1 molecule is significantly smaller than the heterogeneity introduced by the PD-1 molecules (higher α values for PD-L1). BMS-8 interacts more specifically with PD-L1 than with PD-1. More homogeneous surface distribution of the adsorption layer in case of PD-L1 may be caused by formation of homodimer on the electrode surface. Inducing dimerization of PD-L1 protein after interaction with BMS-8 was confirmed by X-ray [30]. On the other hand, experimental data indicate that BMS-8 compound does not bind to PD-1 protein [75]. PD-1 protein also interacts with the electrode, but as a result, the electrode surface is more heterogeneous. Most likely, the interaction of the PD-1 with a modified electrode is probably non-specific and random.

The higher the protein concentration the lower the electric homogeneity at the electrode/electrolyte interface. However, the homogeneity level obtained in the case of anchored PD-L1 proteins at the highest studied concentration 10^{-8} M is unattainable for PD-1, even at the lowest studied concentrations. These differences translate into significant differences between quasi-capacitance of PD-L1 and PD-1 films at the modified electrode surface and demonstrate that BMS-8 strongly and specifically interacts with PD-L1 protein, offering possible routes for PD-L1 assay selectivity in presence of other proteins. The comprehensive impedance analysis allows to qualitatively distinguish PD-L1 and PD-1

MOST WIEDZY Downloaded from mostwiedzy.pl

proteins and provide ultrasensitive quantitative information regarding target protein concentration.

These results are in good agreement with previous studies by the Holak and co-workers, who show that BMS-8 leads to dissociation of PD-1/PD-L1 complex and induction of PD-L1 protein dimerization [28,76]. The interaction of BMS-8 with PD-L1 partially overlaps the hydrophobic interaction surface between PD-1 protein and its ligand, PD-L1. Furthermore, the formation of the homodimer limits access of the PD-1 receptor to the binding site of PD-L1 protein [75–77].

Besides of PD-L1and PD-1 examination, the electrochemical response of other proteins was also investigated to evaluate the electrochemical behavior of the modified electrode on the selectivity of protein detection. For this purpose, we selected CD160, and BTLA proteins that belong to the immunoglobulin-like proteins superfamily (IgSF), the same as PD-L1 and PD-1 [78,79]. It is worth noting that the interaction studies of the BMS-8 molecule with the PD-1 protein have been carried out and the results have shown that BMS-8 binds to PD-L1 but not to PD-1 [28]. In vitro NMR measurements presents that BMS-8 is capable of dissociating the PD-1/PD-L1 interaction in the stoichiometric concentration [75]. The same studies for CD160 and BTLA were not performed. In presented studies, the EIS impedance of selected proteins in 0.01 M PBS, pH 7.0 at concentration of 10^{-8} M was measured. The impedance results in the form of Nyquist plots are shown in Figure S4.

Presented studies show that the functionalized electrodes bind the CD160 and BTLA proteins to the anchored BMS-8 but with significantly less potency than the PD-L1 and PD-1 proteins (Fig. S4). The results of the impedance analysis using R(Q(RW)) EEC are summarized in Table S5.

MOST WIEDZY Downloaded from mostwiedzy.pl

3. Conclusions

Summarizing, this work is focused on designing new assay capable to detect cancer marker, sPD-L1 protein, in low concentration using EIS and CV. It describes the development of the new electrode functionalization, which is capable of PD-L1 detection in PBS solution. The applied approach utilizes the reaction of BMS-8 with cysteamine anchored at gold electrode surface. Performed high-resolution XPS, contact angle, and surface free energy studies confirmed each successful step of the electrode modification. Cyclic voltammetry confirmed the detection of PD-L1 protein in the concentration of 10^{-14} M, while the electrochemical impedance spectroscopy performed at various concentrations in the range of 10^{-18} to 10^{-8} M. We have proved the efficient both PD-L1 as well as PD-1 detection through change in charge transfer resistance R_{CT} even at its lowest concentration of 10^{-18} M. Subsequently, it should be noted that the changes in the electric parameters with PD-L1 and PD-1 concentration show a linear trend, significantly enabling quantitative analysis with the low detection limit of 1.87×10^{-14} for PD-L1 M and 2.93×10^{-14} M for and PD-1 respectively. While offering ultrasensitive protein detection, the R_{CT} analysis does not allow for selective PD-L1 or PD-1 protein determination, since the assay is affected by both proteins. Likely, interaction with PD-L1 is BMS-8 specific while that with PD-1 is guided by less defined surface effects at the functionalized electrode. We claim that the selectivity of the proposed assay may be based on quasi-capacitance parameter analysis. Smaller decrease of electrode homogeneity for PD-L1/BMS-8 interaction in comparison to PD-1/BMS-8 can be explained by dimerization of PD-L1 protein induced by BMS-8 which not occur in case of PD-1/BMS-8. The constant phase element parameters Q and α show that it is possible to differentiate PD-L1 from PD-1 protein and it will be investigating further in more complex mixtures e.g. animal or human serum. Our studies confirmed that immune checkpoint proteins CD160 and BTLA anchor at the electrode with significantly less potency than the PD-L1.

MOST WIEDZY Downloaded from mostwiedzy.pl

538

539 **Acknowledgments**

540 This work was financially supported by Polish National Science Centre (NCN) under
541 Grant No. 2015/17/D/ST5/02571 (J.R.), Grant No. 2017/25/B/NZ1/00827 (G.D.) and by
542 Polpharma Scientific Foundation Grant No. 3/XVIII/2019 (S.R.-M.).

MOST WIEDZY Downloaded from mostwiedzy.pl

References

[1] F. Bray, J. Ferlay, I. Soerjomataram, R.L. Siegel, L.A. Torre, A. Jemal, Global cancer statistics 2018: GLOBOCAN estimates of incidence and mortality worldwide for 36 cancers in 185 countries, CA: A Cancer Journal for Clinicians. 68 (2018) 394–424. https://doi.org/10.3322/caac.21492.

[2] S. Mehta, A. Shelling, A. Muthukaruppan, A. Lasham, C. Blenkiron, G. Laking, C. Print, Predictive and prognostic molecular markers for cancer medicine, Ther Adv Med Oncol. 2 (2010) 125–148. https://doi.org/10.1177/1758834009360519.

[3] R.C. Dolscheid-Pommerich, M. Keyver-Paik, T. Hecking, W. Kuhn, G. Hartmann, B. Stoffel-Wagner, S. Holdenrieder, Clinical performance of LOCI^{TM}-based tumor marker assays for tumor markers CA 15-3, CA 125, CEA, CA 19-9 and AFP in gynecological cancers, Tumour Biol. 39 (2017) 1010428317730246. https://doi.org/10.1177/1010428317730246.

[4] I. Jacobs, R.C. Bast, The CA 125 tumour-associated antigen: a review of the literature, Hum Reprod. 4 (1989) 1–12. https://doi.org/10.1093/oxfordjournals.humrep.a136832.

[5] P.M. Göcze, D.G. Szabó, G.N. Than, I.F. Csaba, K.F. Krommer, Occurrence of CA 125 and CA 19-9 Tumor-Associated Antigens in Sera of Patients with Gynecologic, Trophoblastic, and Colorectal Tumors, GOI. 25 (1988) 268–272. https://doi.org/10.1159/000293797.

[6] X. Frigola, B.A. Inman, C.J. Krco, X. Liu, S.M. Harrington, P.A. Bulur, A.B. Dietz, H. Dong, E.D. Kwon, Soluble B7-H1: Differences in production between dendritic cells and T cells, Immunology Letters. 142 (2012) 78–82. https://doi.org/10.1016/j.imlet.2011.11.001.

[7] J. Zhou, K.M. Mahoney, A. Giobbie-Hurder, F. Zhao, S. Lee, X. Liao, S. Rodig, J. Li, X. Wu, L.H. Butterfield, M. Piesche, M.P. Manos, L.M. Eastman, G. Dranoff, G.J. Freeman, F.S. Hodi, Soluble PD-L1 as a biomarker in malignant melanoma and checkpoint blockade, Cancer Immunol Res. (2017) canimm.0329.2016. https://doi.org/10.1158/2326-6066.CIR-16-0329.

[8] X. Bi, H. Wang, W. Zhang, J. Wang, W. Liu, Z. Xia, H. Huang, W. Jiang, Y. Zhang, L. Wang, PD-L1 is upregulated by EBV-driven LMP1 through NF-κB pathway and correlates with poor prognosis in natural killer/T-cell lymphoma, Journal of Hematology & Oncology. 9 (2016) 109. https://doi.org/10.1186/s13045-016-0341-7.

[9] T. Nagato, T. Ohkuri, K. Ohara, Y. Hirata, K. Kishibe, Y. Komabayashi, S. Ueda, M. Takahara, T. Kumai, K. Ishibashi, A. Kosaka, N. Aoki, K. Oikawa, Y. Uno, N. Akiyama, M. Sado, H. Takei, E. Celis, Y. Harabuchi, H. Kobayashi, Programmed death-ligand 1 and its soluble form are highly expressed in nasal natural killer/T-cell lymphoma: a potential rationale for immunotherapy, Cancer Immunol Immunother. 66 (2017) 877–890. https://doi.org/10.1007/s00262-017-1987-x.

[10] D. Rossille, M. Gressier, D. Damotte, D. Maucort-Boulch, C. Pangault, G. Semana, S. Le Gouill, C. Haioun, K. Tarte, T. Lamy, N. Milpied, T. Fest, Groupe Ouest-Est des Leucémies et Autres Maladies du Sang, Groupe Ouest-Est des Leucémies et Autres Maladies du Sang, High level of soluble programmed cell death ligand 1 in blood impacts overall survival in aggressive diffuse large B-Cell lymphoma: results from a French multicenter clinical trial, Leukemia. 28 (2014) 2367–2375. https://doi.org/10.1038/leu.2014.137.

[11] L. Wang, H. Wang, H. Chen, W. Wang, X. Chen, Q. Geng, Z. Xia, Y. Lu, Serum levels of soluble programmed death ligand 1 predict treatment response and progression free survival in multiple myeloma, Oncotarget. 6 (2015) 41228–41236. https://doi.org/10.18632/oncotarget.5682.

[12] X. Frigola, B.A. Inman, C.M. Lohse, C.J. Krco, J.C. Cheville, R.H. Thompson, B.C. Leibovich, M.L. Blute, H. Dong, E.D. Kwon, Identification of a Soluble Form of B7-H1 That

MOST WIEDZY Downloaded from mostwiedzy.pl

Retains Immunosuppressive Activity and Is Associated with Aggressive Renal Cell Carcinoma, Clin Cancer Res. (2011) clincanres.0250.2010. https://doi.org/10.1158/1078-0432.CCR-10-0250.
[13] S. Kitano, T. Nakayama, M. Yamashita, Biomarkers for Immune Checkpoint Inhibitors in Melanoma, Front. Oncol. 8 (2018). https://doi.org/10.3389/fonc.2018.00270.
[14] S.P. Patel, R. Kurzrock, PD-L1 Expression as a Predictive Biomarker in Cancer Immunotherapy, Mol Cancer Ther. 14 (2015) 847–856. https://doi.org/10.1158/1535-7163.MCT-14-0983.
[15] J.T. Jørgensen, K.B. Nielsen, Companion and complementary diagnostics for first-line immune checkpoint inhibitor treatment in non-small cell lung cancer, Transl Lung Cancer Res. 7 (2018) S95–S99. https://doi.org/10.21037/tlcr.2018.02.08.
[16] C. Teixidó, N. Vilariño, R. Reyes, N. Reguart, PD-L1 expression testing in non-small cell lung cancer, Ther Adv Med Oncol. 10 (2018) 1758835918763493. https://doi.org/10.1177/1758835918763493.
[17] M. Yi, D. Jiao, H. Xu, Q. Liu, W. Zhao, X. Han, K. Wu, Biomarkers for predicting efficacy of PD-1/PD-L1 inhibitors, Molecular Cancer. 17 (2018) 129. https://doi.org/10.1186/s12943-018-0864-3.
[18] J. He, Y. Pan, Y. Guo, B. Li, Y. Tang, Study on the Expression Levels and Clinical Significance of PD-1 and PD-L1 in Plasma of NSCLC Patients, Journal of Immunotherapy. 43 (2020) 156–164. https://doi.org/10.1097/CJI.0000000000000315.
[19] J. Zhou, K.M. Mahoney, A. Giobbie-Hurder, F. Zhao, S. Lee, X. Liao, S. Rodig, J. Li, X. Wu, L.H. Butterfield, M. Piesche, M.P. Manos, L.M. Eastman, G. Dranoff, G.J. Freeman, F.S. Hodi, Soluble PD-L1 as a biomarker in malignant melanoma and checkpoint blockade, Cancer Immunol Res. (2017) canimm.0329.2016. https://doi.org/10.1158/2326-6066.CIR-16-0329.
[20] D. Rossille, M. Gressier, D. Damotte, D. Maucort-Boulch, C. Pangault, G. Semana, S. Le Gouill, C. Haioun, K. Tarte, T. Lamy, N. Milpied, T. Fest, Groupe Ouest-Est des Leucémies et Autres Maladies du Sang, Groupe Ouest-Est des Leucémies et Autres Maladies du Sang, High level of soluble programmed cell death ligand 1 in blood impacts overall survival in aggressive diffuse large B-Cell lymphoma: results from a French multicenter clinical trial, Leukemia. 28 (2014) 2367–2375. https://doi.org/10.1038/leu.2014.137.
[21] L. Wang, H. Wang, H. Chen, W. Wang, X. Chen, Q. Geng, Z. Xia, Y. Lu, Serum levels of soluble programmed death ligand 1 predict treatment response and progression free survival in multiple myeloma, Oncotarget. 6 (2015) 41228–41236. https://doi.org/10.18632/oncotarget.5682.
[22] Y. Li, Y. Li, Y. Xiao, Y. Xiao, M. Su, M. Su, R. Zhang, R. Zhang, J. Ding, J. Ding, X. Hao, X. Hao, Y. Ma, Y. Ma, Role of soluble programmed death-1 (sPD-1) and sPD-ligand 1 in patients with cystic echinococcosis, Experimental and Therapeutic Medicine. 11 (2016) 251–256. https://doi.org/10.3892/etm.2015.2876.
[23] L.S. Chupak, M. Ding, S.W. Martin, X. Zheng, P. Hewawasam, T.P. Connolly, N. Xu, K.-S. Yeung, J. Zhu, D.R. Langley, D.J. TENNEY, P.M. Scola, Compounds useful as immunomodulators, WO2015160641A2, 2015. https://patents.google.com/patent/WO2015160641A2/en?oq=WO+2015%2f160641+A2.+WO+2015%2f160641+A2 (accessed January 18, 2019).
[24] L.S. Chupak, X. Zheng, Compounds useful as immunomodulators, WO2015034820A1, 2015. https://patents.google.com/patent/WO2015034820A1/en?oq=WO+2015%2f034820+A1.+WO2015034820+A1 (accessed January 18, 2019).
[25] M.J. Aghajani, T.L. Roberts, T. Yang, C.E. McCafferty, N.J. Caixeiro, P. DeSouza, N. Niles, Elevated levels of soluble PD-L1 are associated with reduced recurrence in papillary

MOST WIEDZY Downloaded from mostwiedzy.pl

thyroid cancer, Endocrine Connections. 8 (2019) 1040–1051. https://doi.org/10.1530/EC-19-0210.
[26] Y. Ding, C. Sun, J. Li, L. Hu, M. Li, J. Liu, L. Pu, S. Xiong, The Prognostic Significance of Soluble Programmed Death Ligand 1 Expression in Cancers: A Systematic Review and Meta-analysis, Scandinavian Journal of Immunology. 86 (2017) 361–367. https://doi.org/10.1111/sji.12596.
[27] X. Wu, L. Xu, Q. Cheng, L. Nie, S. Zhang, Y. Du, J. Xue, Increased serum soluble programmed death ligand 1(sPD-L1) is associated with the presence of interstitial lung disease in rheumatoid arthritis: A monocentric cross-sectional study, Respiratory Medicine. 166 (2020) 105948. https://doi.org/10.1016/j.rmed.2020.105948.
[28] L. Skalniak, K.M. Zak, K. Guzik, K. Magiera, B. Musielak, M. Pachota, B. Szelazek, J. Kocik, P. Grudnik, M. Tomala, S. Krzanik, K. Pyrc, A. Dömling, G. Dubin, T.A. Holak, Small-molecule inhibitors of PD-1/PD-L1 immune checkpoint alleviate the PD-L1-induced exhaustion of T-cells, Oncotarget. 8 (2017) 72167–72181. https://doi.org/10.18632/oncotarget.20050.
[29] U. Jarocka, R. Sawicka, A. Góra-Sochacka, A. Sirko, W. Zagórski-Ostoja, J. Radecki, H. Radecka, Electrochemical immunosensor for detection of antibodies against influenza A virus H5N1 in hen serum, Biosensors and Bioelectronics. 55 (2014) 301–306. https://doi.org/10.1016/j.bios.2013.12.030.
[30] K.M. Zak, P. Grudnik, K. Guzik, B.J. Zieba, B. Musielak, A. Dömling, G. Dubin, T.A. Holak, Structural basis for small molecule targeting of the programmed death ligand 1 (PD-L1), Oncotarget. 7 (2016) 30323–30335. https://doi.org/10.18632/oncotarget.8730.
[31] A. Zielinski, M. Cieslik, M. Sobaszek, R. Bogdanowicz, K. Darowicki, J. Ryl, Multifrequency nanoscale impedance microscopy (m-NIM): A novel approach towards detection of selective and subtle modifications on the surface of polycrystalline boron-doped diamond electrodes, Ultramicroscopy. 199 (2019) 34–45. https://doi.org/10.1016/j.ultramic.2019.01.004.
[32] A. Mezni, M.M. Ibrahim, M. El-Kemary, A.A. Shaltout, N.Y. Mostafa, J. Ryl, T. Kumeria, T. Altalhi, M.A. Amin, Cathodically activated Au/TiO2 nanocomposite synthesized by a new facile solvothermal method: An efficient electrocatalyst with Pt-like activity for hydrogen generation, Electrochimica Acta. 290 (2018) 404–418. https://doi.org/10.1016/j.electacta.2018.08.083.
[33] J. Kloubek, Development of methods for surface free energy determination using contact angles of liquids on solids, Advances in Colloid and Interface Science. 38 (1992) 99–142. https://doi.org/10.1016/0001-8686(92)80044-X.
[34] C.J. van Oss, Acid—base interfacial interactions in aqueous media, Colloids and Surfaces A: Physicochemical and Engineering Aspects. 78 (1993) 1–49. https://doi.org/10.1016/0927-7757(93)80308-2.
[35] D.K. Owens, R.C. Wendt, Estimation of the surface free energy of polymers, Journal of Applied Polymer Science. 13 (1969) 1741–1747. https://doi.org/10.1002/app.1969.070130815.
[36] T. Swebocki, P. Niedziałkowski, A. Cirocka, E. Szczepańska, T. Ossowski, A. Wcisło, In pursuit of key features for constructing electrochemical biosensors – electrochemical and acid-base characteristic of self-assembled monolayers on gold, Supramolecular Chemistry. 0 (2020) 1–11. https://doi.org/10.1080/10610278.2020.1739685.
[37] S. Shahrokhian, A. Mahdavi-Shakib, M. Ghalkhani, R. Saberi, Gold Electrode Modified with Self-Assembled Monolayer of Cysteamine-Functionalized MWCNT and Its Application in Simultaneous Determination of Dopamine and Uric Acid, Electroanalysis. 24 (2012) 425–432. https://doi.org/10.1002/elan.201100545.
[38] C. Poitras, N. Tufenkji, A QCM-D-based biosensor for E. coli O157:H7 highlighting

MOST WIEDZY Downloaded from mostwiedzy.pl

692 the relevance of the dissipation slope as a transduction signal, Biosensors and Bioelectronics.
693 24 (2009) 2137–2142. https://doi.org/10.1016/j.bios.2008.11.016.
694 [39] Y. Zhang, Y. Li, W. Wu, Y. Jiang, B. Hu, Chitosan coated on the layers' glucose
695 oxidase immobilized on cysteamine/Au electrode for use as glucose biosensor, Biosensors
696 and Bioelectronics. 60 (2014) 271–276. https://doi.org/10.1016/j.bios.2014.04.035.
697 [40] R.K. Shervedani, S.A. Mozaffari, Copper(II) Nanosensor Based on a Gold Cysteamine
698 Self-Assembled Monolayer Functionalized with Salicylaldehyde, Anal. Chem. 78 (2006)
699 4957–4963. https://doi.org/10.1021/ac052292y.
700 [41] R.K. Shervedani, M. Bagherzadeh, S.A. Mozaffari, Determination of dopamine in the
701 presence of high concentration of ascorbic acid by using gold cysteamine self-assembled
702 monolayers as a nanosensor, Sensors and Actuators B: Chemical. 115 (2006) 614–621.
703 https://doi.org/10.1016/j.snb.2005.10.027.
704 [42] W.X. Cheng, D.Y. Peng, C.H. Lu, C.W. Fang, Direct electrochemical behavior of the
705 Cysteamine/DNA/SWNTs-film-modified Au electrode and its interaction with taxol, Russ J
706 Electrochem. 44 (2008) 1052–1057. https://doi.org/10.1134/S1023193508090103.
707 [43] K. De Wael, H. Buschop, L. De Smet, A. Adriaens, Immobilization of cytochrome c
708 on cysteamine-modified gold electrodes with EDC as coupling agent, Talanta. 76 (2008) 309–
709 313. https://doi.org/10.1016/j.talanta.2008.02.040.
710 [44] G.-Z. Garyfallou, O. Ketebu, S. Şahin, E.B. Mukaetova-Ladinska, M. Catt, E.H. Yu,
711 Electrochemical Detection of Plasma Immunoglobulin as a Biomarker for Alzheimer's
712 Disease, Sensors. 17 (2017) 2464. https://doi.org/10.3390/s17112464.
713 [45] M.M.S. Silva, I.T. Cavalcanti, M.F. Barroso, M.G.F. Sales, R.F. Dutra, Gold electrode
714 modified by self-assembled monolayers of thiols to determine DNA sequences hybridization,
715 J Chem Sci. 122 (2010) 911–917. https://doi.org/10.1007/s12039-010-0079-7.
716 [46] M. Wirde, U. Gelius, L. Nyholm, Self-Assembled Monolayers of Cystamine and
717 Cysteamine on Gold Studied by XPS and Voltammetry, Langmuir. 15 (1999) 6370–6378.
718 https://doi.org/10.1021/la9903245.
719 [47] K. Malecka, L. Michalczuk, H. Radecka, J. Radecki, Ion-Channel Genosensor for the
720 Detection of Specific DNA Sequences Derived from Plum Pox Virus in Plant Extracts,
721 Sensors. 14 (2014) 18611–18624. https://doi.org/10.3390/s141018611.
722 [48] G. Ilangovan, K. Chandrasekara Pillai, Electrochemical and XPS Characterization of
723 Glassy Carbon Electrode Surface Effects on the Preparation of a Monomeric Molybdate(VI)-
724 Modified Electrode, Langmuir. 13 (1997) 566–575. https://doi.org/10.1021/la960053n.
725 [49] J. Ryl, L. Burczyk, R. Bogdanowicz, M. Sobaszek, K. Darowicki, Study on surface
726 termination of boron-doped diamond electrodes under anodic polarization in H2SO4 by
727 means of dynamic impedance technique, Carbon. 96 (2016) 1093–1105.
728 https://doi.org/10.1016/j.carbon.2015.10.064.
729 [50] M. Sobaszek, K. Siuzdak, J. Ryl, M. Sawczak, S. Gupta, S.B. Carrizosa, M. Ficek, B.
730 Dec, K. Darowicki, R. Bogdanowicz, Diamond Phase (sp3-C) Rich Boron-Doped Carbon
731 Nanowalls (sp2-C): Physicochemical and Electrochemical Properties, J. Phys. Chem. C. 121
732 (2017) 20821–20833. https://doi.org/10.1021/acs.jpcc.7b06365.
733 [51] M. Ficek, K.J. Sankaran, J. Ryl, R. Bogdanowicz, I.-N. Lin, K. Haenen, K. Darowicki,
734 Ellipsometric investigation of nitrogen doped diamond thin films grown in microwave
735 CH4/H2/N2 plasma enhanced chemical vapor deposition, Appl. Phys. Lett. 108 (2016)
736 241906. https://doi.org/10.1063/1.4953779.
737 [52] J. Wysocka, M. Cieslik, S. Krakowiak, J. Ryl, Carboxylic acids as efficient corrosion
738 inhibitors of aluminium alloys in alkaline media, Electrochimica Acta. 289 (2018) 175–192.
739 https://doi.org/10.1016/j.electacta.2018.08.070.
740 [53] J. Wysocka, S. Krakowiak, J. Ryl, Evaluation of citric acid corrosion inhibition
741 efficiency and passivation kinetics for aluminium alloys in alkaline media by means of

MOST WIEDZY Downloaded from mostwiedzy.pl

dynamic impedance monitoring, Electrochimica Acta. 258 (2017) 1463–1475. https://doi.org/10.1016/j.electacta.2017.12.017.
[54] Q. Liu, X. Tong, G. Zhou, H2O Dissociation-Induced Aluminum Oxide Growth on Oxidized Al(111) Surfaces, Langmuir. 31 (2015) 13117–13126. https://doi.org/10.1021/acs.langmuir.5b02769.
[55] P. Niedziałkowski, R. Bogdanowicz, P. Zięba, J. Wysocka, J. Ryl, M. Sobaszek, T. Ossowski, Melamine-modified Boron-doped Diamond towards Enhanced Detection of Adenine, Guanine and Caffeine, Electroanalysis. 28 (2016) 211–221. https://doi.org/10.1002/elan.201500528.
[56] P. Niedziałkowski, T. Ossowski, P. Zięba, A. Cirocka, P. Rochowski, S.J. Pogorzelski, J. Ryl, M. Sobaszek, R. Bogdanowicz, Poly-l-lysine-modified boron-doped diamond electrodes for the amperometric detection of nucleic acid bases, Journal of Electroanalytical Chemistry. 756 (2015) 84–93. https://doi.org/10.1016/j.jelechem.2015.08.006.
[57] J.-B. Jorcin, M.E. Orazem, N. Pébère, B. Tribollet, CPE analysis by local electrochemical impedance spectroscopy, Electrochimica Acta. 51 (2006) 1473–1479. https://doi.org/10.1016/j.electacta.2005.02.128.
[58] P. Zoltowski, On the electrical capacitance of interfaces exhibiting constant phase element behaviour, Journal of Electroanalytical Chemistry. 443 (1998) 149–154. https://doi.org/10.1016/S0022-0728(97)00490-7.
[59] P. Córdoba-Torres, T.J. Mesquita, O. Devos, B. Tribollet, V. Roche, R.P. Nogueira, On the intrinsic coupling between constant-phase element parameters α and Q in electrochemical impedance spectroscopy, Electrochimica Acta. 72 (2012) 172–178. https://doi.org/10.1016/j.electacta.2012.04.020.
[60] R.K. Shervedani, S.A. Mozaffari, Impedimetric sensing of uranyl ion based on phosphate functionalized cysteamine self-assembled monolayers, Analytica Chimica Acta. 562 (2006) 223–228. https://doi.org/10.1016/j.aca.2006.01.046.
[61] J. Wysocka, M. Cieslik, S. Krakowiak, J. Ryl, Carboxylic acids as efficient corrosion inhibitors of aluminium alloys in alkaline media, Electrochimica Acta. 289 (2018) 175–192. https://doi.org/10.1016/j.electacta.2018.08.070.
[62] P. Niedzialkowski, P. Slepski, J. Wysocka, J. Chamier-Cieminska, L. Burczyk, M. Sobaszek, A. Wcislo, T. Ossowski, R. Bogdanowicz, J. Ryl, Multisine impedimetric probing of biocatalytic reactions for label-free detection of DEFB1 gene: How to verify that your dog is not human?, Sensors and Actuators B: Chemical. 323 (2020) 128664. https://doi.org/10.1016/j.snb.2020.128664.
[63] R.K. Shervedani, S.A. Mozaffari, Impedimetric sensing of uranyl ion based on phosphate functionalized cysteamine self-assembled monolayers, Analytica Chimica Acta. 562 (2006) 223–228. https://doi.org/10.1016/j.aca.2006.01.046.
[64] N. Borghol, L. Mora, T. Jouenne, N. Jaffézic-Renault, N. Sakly, A.C. Duncan, Y. Chevalier, P. Lejeune, A. Othmane, Monitoring of E. coli immobilization on modified gold electrode: A new bacteria-based glucose sensor, Biotechnol Bioproc E. 15 (2010) 220–228. https://doi.org/10.1007/s12257-009-0146-4.
[65] C. Tlili, E. Sokullu, M. Safavieh, M. Tolba, M.U. Ahmed, M. Zourob, Bacteria Screening, Viability, And Confirmation Assays Using Bacteriophage-Impedimetric/Loop-Mediated Isothermal Amplification Dual-Response Biosensors, Anal. Chem. 85 (2013) 4893–4901. https://doi.org/10.1021/ac302699x.
[66] P. Hashemi, A. Afkhami, H. Bagheri, S. Amidi, T. Madrakian, Fabrication of a novel impedimetric sensor based on l-Cysteine/Cu(II) modified gold electrode for sensitive determination of ampyra, Analytica Chimica Acta. 984 (2017) 185–192. https://doi.org/10.1016/j.aca.2017.06.038.
[67] R.K. Shervedani, A. Farahbakhsh, M. Bagherzadeh, Functionalization of gold

MOST WIEDZY Downloaded from mostwiedzy.pl

cysteamine self-assembled monolayer with ethylenediaminetetraacetic acid as a novel nanosensor, Analytica Chimica Acta. 587 (2007) 254–262. https://doi.org/10.1016/j.aca.2007.01.053.
[68] R.K. Shervedani, M. Bagherzadeh, S.A. Mozaffari, Determination of dopamine in the presence of high concentration of ascorbic acid by using gold cysteamine self-assembled monolayers as a nanosensor, Sensors and Actuators B: Chemical. 115 (2006) 614–621. https://doi.org/10.1016/j.snb.2005.10.027.
[69] R.K. Shervedani, S.A. Mozaffari, Copper(II) Nanosensor Based on a Gold Cysteamine Self-Assembled Monolayer Functionalized with Salicylaldehyde, Anal. Chem. 78 (2006) 4957–4963. https://doi.org/10.1021/ac052292y.
[70] Z. Li, L. Zhang, H. Mo, Y. Peng, H. Zhang, Z. Xu, C. Zheng, Z. Lu, Size-fitting effect for hybridization of DNA/mercaptohexanol mixed monolayers on gold, Analyst. 139 (2014) 3137–3145. https://doi.org/10.1039/C4AN00280F.
[71] M. Tolba, M.U. Ahmed, C. Tlili, F. Eichenseher, M.J. Loessner, M. Zourob, A bacteriophage endolysin-based electrochemical impedance biosensor for the rapid detection of Listeria cells, Analyst. 137 (2012) 5749–5756. https://doi.org/10.1039/C2AN35988J.
[72] H. Xiang, Y. Wang, M. Wang, Y. Shao, Y. Jiao, Y. Zhu, A redox cycling-amplified electrochemical immunosensor for α-fetoprotein sensitive detection via polydopamine nanolabels, Nanoscale. 10 (2018) 13572–13580. https://doi.org/10.1039/C8NR02946F.
[73] K. Siuzdak, P. Niedziałkowski, M. Sobaszek, T. Łęga, M. Sawczak, E. Czaczyk, K. Dziąbowska, T. Ossowski, D. Nidzworski, R. Bogdanowicz, Biomolecular influenza virus detection based on the electrochemical impedance spectroscopy using the nanocrystalline boron-doped diamond electrodes with covalently bound antibodies, Sensors and Actuators B: Chemical. 280 (2019) 263–271. https://doi.org/10.1016/j.snb.2018.10.005.
[74] D. Nidzworski, K. Siuzdak, P. Niedziałkowski, R. Bogdanowicz, M. Sobaszek, J. Ryl, P. Weiher, M. Sawczak, E. Wnuk, W.A. Goddard, A. Jaramillo-Botero, T. Ossowski, A rapid-response ultrasensitive biosensor for influenza virus detection using antibody modified boron-doped diamond, Scientific Reports. 7 (2017) 15707. https://doi.org/10.1038/s41598-017-15806-7.
[75] K.M. Zak, P. Grudnik, K. Guzik, B.J. Zieba, B. Musielak, A. Dömling, G. Dubin, T.A. Holak, Structural basis for small molecule targeting of the programmed death ligand 1 (PD-L1), Oncotarget. 7 (2016) 30323–30335. https://doi.org/10.18632/oncotarget.8730.
[76] K.M. Zak, P. Grudnik, K. Magiera, A. Dömling, G. Dubin, T.A. Holak, Structural Biology of the Immune Checkpoint Receptor PD-1 and Its Ligands PD-L1/PD-L2, Structure. 25 (2017) 1163–1174. https://doi.org/10.1016/j.str.2017.06.011.
[77] D. Shi, X. An, Q. Bai, Z. Bing, S. Zhou, H. Liu, X. Yao, Computational Insight Into the Small Molecule Intervening PD-L1 Dimerization and the Potential Structure-Activity Relationship, Front. Chem. 7 (2019). https://doi.org/10.3389/fchem.2019.00764.
[78] W. Liu, S.C. Garrett, E.V. Fedorov, U.A. Ramagopal, S.J. Garforth, J.B. Bonanno, S.C. Almo, Structural Basis of CD160:HVEM Recognition, Structure. (2019). https://doi.org/10.1016/j.str.2019.05.010.
[79] R.J. Greenwald, G.J. Freeman, A.H. Sharpe, The B7 Family Revisited, Annual Review of Immunology. 23 (2005) 515–548. https://doi.org/10.1146/annurev.immunol.23.021704.115611.

MOST WIEDZY Downloaded from mostwiedzy.pl